

Collapse and Expansion of Scalar Thin-Shell for a Class of Black Holes

M. Sharif ^{*} and Faisal Javed [†]

Department of Mathematics, University of the Punjab,
Quaid-e-Azam Campus, Lahore-54590, Pakistan.

Abstract

This paper investigates the dynamics of thin-shell in the presence of perfect fluid as well as scalar field. We formulate the equations of motion using Israel thin-shell formalism by taking the interior and exterior regions of Schwarzschild, Kerr as well as Kerr-Newmann black hole. We find numerical solutions of equations of motion and effective potential to analyze the scalar shell for collapse and expansion. It is found that the rate of collapse and expansion of scalar shell through shell's radius depends on charge and rotation parameters. We conclude that the massive scalar shell leads to collapse of thin-shell, while massless scalar shell indicates both collapse as well as expansion.

Keywords: Gravitational collapse; Scalar field; Israel thin-shell formalism.

PACS: 04.20.-q; 04.40.Dg; 04.70.Bw; 75.78.-n

1 Introduction

Geon is a notion of electromagnetic-gravitational field that is held together in a confined region due its own gravity. This entity was introduced by Wheeler et al. [1] who established particle-like solutions from classical electromagnetic field coupled to general relativity. They used the resulting solutions to analyze the scalar field. Bergmann and Leipnik [2] studied solutions of the field

^{*}msharif.math@pu.edu.pk

[†]faisalrandawa@hotmail.com

equations in the presence of scalar field for Schwarzschild black hole (BH). In general relativity, scalar field appears in the low energy limit of string theory [3]. There is no experimental evidence for the existence of such particles that are associated with the scalar field. Harada et al. [4] studied that gravitational collapse of compact objects in scalar-tensor theories predict scalar field as a source of gravitational waves that can be identified by the advanced detectors.

The study of cosmological as well as astrophysical objects composed of scalar field has been the subject of great interest for many researchers. Kaup [5] was the pioneer to investigate the geometrical configuration for complex massive scalar field. Ruffini and Bonazzola [6] examined spherical geometries and found the equilibrium conditions for boson stars solutions. Seidel and Suen [7] studied the dynamical evolution of compact stars associated with scalar field and found that boson stars have stable configurations for several values of the scalar fields. These results provide information corresponding to existence as well as formation of boson stars. Jetzer [8] investigated the equilibrium configuration of boson stars and discussed their dynamical instability. Many people [9] investigated the nature of spacetime singularity for massless scalar field with spherical geometry. Siebel et al. [10] analyzed self-gravitating objects composed of massless scalar field and found that boson stars either oscillate or undergo collapse to form a BH. Bhattacharya et al. [11] studied the collapse of spherical stars associated with massless scalar field and examined appropriate condition for the existence of a class of non-singular models.

The smooth matching of interior and exterior spacetimes helps to evaluate exact solutions of the field equations. This is also a key aspect to study the boundary of BHs, gravitational waves and contribution of matter at thin-shell. Israel [12] developed thin-shell formalism to investigate the dynamics of fluid configuration at thin-shell. It is observed that the presence of thin layer of matter at thin-shell leads to jump discontinuity across the boundary of interior and exterior regions. In order to analyze thin-shell, Israel formalism has widely been used [13].

De La Cruz and Israel [14] generalized Israel thin-shell formalism for charged thin-shell in the absence of pressure. Kuchar [15] examined the charged thin-shell problem by considering polytropic equation of state (EoS). Chase [16] investigated the instability of spherically symmetric charged fluid shell. Boulware [17] analyzed charged thin-shell and found that collapse produces a naked singularity when matter (with negative density) is located at

thin-shell. Núñez [18] studied spherically symmetric massive shell and found that the shell oscillates radially around a central compact object. Núñez et al. [19] analyzed the effect of scalar field for Schwarzschild BH and found that massive scalar field leads to collapse of the shell when both pressure and gravitational mass are proportional. Pereira and Wang [20] used thin-shell formalism to study the non-rotating shell constructed from two cylindrical regions and observed the behavior of collapsing shell. Sharif and his collaborators [21] used this formalism to investigate spherical as well as planar collapse. Sharif and Abbas [22] explored the dynamics of charged scalar thin-shell and concluded that for both (massless and massive scalar fields) shell can expand to infinity or collapse to zero size forming a curvature singularity. Sharif and Iftikhar [23] explored a class of regular BHs and found that massless scalar shell leads to expansion, collapse and equilibrium structure while the massive case leads to collapse only.

This work is devoted to study the effect of scalar field on the dynamics of thin-shell using Israel formalism for a class of BHs. The paper is organized as follows. In section **2**, we construct the equations of motion by applying Israel thin-shell formalism for Schwarzschild, Kerr and Kerr-Newmann BHs. Section **3** explores massless and massive scalar fields to investigate these equations of motion. Finally, we summarize our results in the last section.

2 Equations of Motion

In this section, we construct thin-shell for Schwarzschild, Kerr and Kerr-Newmann BHs. We consider a hypersurface (Σ) that divides a spherically symmetric spacetime into two four-dimensional manifolds N^+ and N^- representing interior and exterior regions, respectively. The line element for interior and exterior regions of the Schwarzschild, Kerr and Kerr-Newmann BHs is given as

$$\begin{aligned}
 ds_{\pm}^2 = & -F_{\pm}(R)dt^2 - \left(\frac{4m_{\pm}R}{A} - \frac{2Q_{\pm}^2}{A} \right) a \sin^2 \theta dt d\phi + \left(\frac{A}{B} \right) dr^2 + Ad\theta^2 \\
 & + \left(R^2 + a^2 + \frac{2m_{\pm}a^2R \sin^2 \theta}{A} - \frac{a^2Q_{\pm}^2 \sin^2 \theta}{A} \right) \sin^2 \theta d\phi^2, \quad (1)
 \end{aligned}$$

where

$$A = R^2 + a^2 \cos^2 \theta, \quad B = R^2 - 2m_{\pm}R + a^2 + Q_{\pm}^2,$$

here m_{\pm} , Q_{\pm} and a denote the mass, charge and rotation parameters, respectively. Moreover, we assume that interior region contains more mass than the exterior region, i.e., $m_+ \neq m_-$, while the charge is uniformly distributed in both regions, i.e., $Q_+ = Q_- = Q$. The explicit forms of the defining parameters corresponding to different BHs are given in Table 1.

Table 1: A Class of BHs.

Name of BH	$F(R)$
Schwarzschild	$F_{\pm 1}(R) = \left(1 - \frac{2m_{\pm}}{R}\right)$, $a = 0$, $Q_{\pm} = 0$
Kerr	$F_{\pm 2}(R) = \left(1 - \frac{2m_{\pm}R}{A}\right)$, $Q_{\pm} = 0$
Kerr-Newmann	$F_{\pm 3}(R) = \left(1 - \frac{2m_{\pm}R}{A} + \frac{Q_{\pm}^2}{A}\right)$

We apply the intrinsic coordinates $\xi^i = (\tau, \theta, \phi)$ over Σ at $R = R(\tau)$. Consequently, Eq.(1) yields

$$\begin{aligned}
 ds_{\pm}^2 &= \left[-F_{\pm}(R) + \frac{A}{B} \left(\frac{dR}{d\tau} \right)^2 \left(\frac{d\tau}{dt} \right)^2 \right] dt^2 - \left(\frac{4m_{\pm}R}{A} - \frac{2Q_{\pm}^2}{A} \right) a \sin^2 \theta d\phi dt \\
 &+ Ad\theta^2 + \left(R^2 + a^2 + \frac{2m_{\pm}a^2R \sin^2 \theta}{A} - \frac{a^2Q_{\pm}^2 \sin^2 \theta}{A} \right) \sin^2 \theta d\phi^2, \quad (2)
 \end{aligned}$$

where τ is the proper time. The corresponding induced metric for hypersurface is defined as

$$ds^2 = -d\tau^2 + R^2(\tau) (d\theta^2 + \sin^2 \theta d\phi^2). \quad (3)$$

Comparing Eqs.(2) and (3), we obtain

$$\left[F_{\pm}(R) - \frac{A}{B} \left(\frac{dR}{d\tau} \right)^2 \left(\frac{d\tau}{dt} \right)^2 \right]^{\frac{1}{2}} dt = (d\tau)_{\Sigma}.$$

The outward unit normals n_{α}^{\pm} corresponding to interior as well as exterior

region are $n_\alpha^\pm = (n_0, n_1, 0, 0)$, where

$$\begin{aligned}
n_0 &= -\dot{R} \left(\frac{B + A\dot{R}^2}{BF_\pm} \right)^{-\frac{1}{2}} \left[\frac{B}{A} + \left\{ AB\dot{R}^2 F_\pm (-A(a^2 + R^2) + a^2 \sin^2 \theta) \right. \right. \\
&\quad \times (Q^2 - 2m_\pm R) \left. \left. \right\} \left\{ (B + A\dot{R}^2) (A^2 F_\pm (a^2 + R^2) - a^2 (Q^2 - 2m_\pm R)) \right. \right. \\
&\quad \times (AF_\pm - 4Q^2 + 8m_\pm R) \sin^2 \theta \left. \left. \right\}^{-1} \right]^{-\frac{1}{2}}, \\
n_1 &= \left[\frac{B}{A} + \left\{ AB\dot{R}^2 F_\pm (-A(a^2 + R^2) + a^2 \sin^2 \theta (Q^2 - 2m_\pm R)) \right\} \right. \\
&\quad \times \left\{ (B + A\dot{R}^2) (A^2 F_\pm (a^2 + R^2) - a^2 (Q^2 - 2m_\pm R)) \right. \\
&\quad \times (AF_\pm - 4Q^2 + 8m_\pm R) \sin^2 \theta \left. \left. \right\}^{-1} \right]^{-\frac{1}{2}}.
\end{aligned}$$

Here, dot denotes derivative with respect to τ . The extrinsic curvatures joining two sides of the shell are defined as

$$K_{ij}^\pm = -n_\beta^\pm \left(\frac{d^2 x_\pm^\beta}{d\xi^i d\xi^j} + \Gamma_{\mu\nu}^\beta \frac{dx_\pm^\mu dx_\pm^\nu}{d\xi^i d\xi^j} \right), \quad \mu, \nu, \beta = 0, 1, 2, 3. \quad (4)$$

The discontinuity of extrinsic curvature appears due to the existence of thin layer of matter on Σ . The dynamics of this thin-shell is observed by using the field equations at Σ , i.e., by the Lanczos equations

$$S_{ij} = \frac{1}{8\pi} \{g_{ij}K - [K_{ij}]\}, \quad i, j = 0, 2, 3, \quad (5)$$

where $[K_{ij}] = K_{ij}^+ - K_{ij}^-$ and $K = tr[K_{ij}] = [K_i^i]$. The Lanczos equations for spherical thin-shell reduces to

$$\sigma = \frac{-1}{4\pi} [K_\theta^\theta], \quad p = \frac{1}{8\pi} \{[K_\tau^\tau] + [K_\theta^\theta]\}. \quad (6)$$

In the absence of surface energy density (σ) and pressure (p), the connection between these geometries is referred as a boundary surface, otherwise it is known as thin-shell. The corresponding surface energy density can be

expressed as

$$\begin{aligned} \sigma &= \frac{B}{8\pi r A} \left[\frac{B}{A} + \left\{ AB\dot{R}^2 F_{\pm} (-A(a^2 + R^2) + a^2 \sin^2 \theta (Q^2 - 2m_{\pm}R)) \right\} \right. \\ &\times \left\{ (B + A\dot{R}^2) (A^2 F_{\pm} (a^2 + R^2) - a^2 (Q^2 - 2m_{\pm}R)) \right. \\ &\times \left. \left. (AF_{\pm} - 4Q^2 + 8m_{\pm}R) \sin^2 \theta \right\}^{-1} \right]^{-\frac{1}{2}}. \end{aligned} \quad (7)$$

The above equation can be rewritten as

$$\dot{R}^2 + V_{eff}(R) = 0, \quad (8)$$

where

$$\begin{aligned} V_{eff}(R) &= \left\{ B (B - 64A\pi^2 r^2 \sigma^2) (-A^2 F_{\pm} (a^2 + r^2) + a^2 (Q^2 - 2m_{\pm}r)) \right. \\ &\times (AF_{\pm} - 4Q^2 + 8m_{\pm}r) \sin^2 \theta \left. \right\} \left\{ A^3 B F_{\pm} (a^2 + r^2) - a^2 A \right. \\ &\times (Q^2 - 2m_{\pm}r) (B (AF_{\pm} - 4Q^2 + 8m_{\pm}r) + 256A\pi^2 r^2 \\ &\times (Q^2 - 2m_{\pm}r) \sigma^2) \sin^2 \theta \left. \right\}^{-1}. \end{aligned} \quad (9)$$

It is observed that Eq.(8) satisfies the energy conservation law, i.e., the sum of the component of kinetic (\dot{R}^2) and potential ($V_{eff}(R)$) energies vanishes at any time. The effective potential for Schwarzschild, Kerr and Kerr-Newmann BHs turns out to be

$$V_{eff1}(R) = -F_{\pm 1} + 16\pi^2 R^2 \sigma^2, \quad (10)$$

$$\begin{aligned} V_{eff2}(R) &= \left\{ B (B - 16A\pi^2 R^2 \sigma^2) (A^2 F_{\pm 2} (a^2 + R^2) + 2a^2 m_{\pm} R (AF_{\pm 2} \right. \\ &+ 8m_{\pm} R) \sin^2 \theta) \left. \right\} \left\{ A^3 B F_{\pm 2} (a^2 + R^2) + 2a^2 A m_{\pm} R (ABF_{\pm 2} \right. \\ &+ 8Bm_{\pm} R - 128Am_{\pm}\pi^2 R^3 \sigma^2) \sin^2 \theta \left. \right\}^{-1}, \end{aligned} \quad (11)$$

$$\begin{aligned} V_{eff3}(R) &= \left\{ (B(B - 64A\pi^2 R^2 \sigma^2) (-A^2 F_{\pm 3} (a^2 + R^2) + a^2 (Q^2 - 2m_{\pm}R)) \right. \\ &\times (AF_{\pm 3} - 4Q^2 + 8m_{\pm}R) \sin^2 \theta) \left. \right\} \left\{ (A^3 B F_{\pm 3} (a^2 + R^2) - a^2 A \right. \\ &\times (Q^2 - 2m_{\pm}R) (B (AF_{\pm 3} - 4Q^2 + 8m_{\pm}R) + 256A\pi^2 R^2 \\ &\times (Q^2 - 2m_{\pm}R) \sigma^2) \sin^2 \theta \left. \right\}^{-1}. \end{aligned} \quad (12)$$

3 Analysis of Equations of Motion

Here we investigate the scalar shell and its dynamical behavior for a class of BHs. We evaluate velocity of the scalar shell and its effective potential with

respect to stationary observer. Also, we discuss the effect of charge as well as rotation parameter on the motion of scalar shell. For this purpose, we formulate a relation between surface energy density and the mass of thin-shell. The surface energy density and pressure follow the conservation equation

$$p \frac{d\Delta}{d\tau} + \frac{d}{d\tau}(\sigma\Delta) = 0, \quad (13)$$

where $\Delta = 4\pi R^2$ represents area of the shell. Consequently, the conservation equation for $p = p(\sigma, R)$ takes the form

$$\sigma' + \frac{2}{R} [\sigma + p(\sigma, R)] = 0. \quad (14)$$

This equation can be solved by using EoS, $p = k\sigma$, yielding

$$\sigma = \sigma_0 \left(\frac{R_0}{R} \right)^{2(k+1)}, \quad (15)$$

where k is a constant and R_0 represents initial position of the shell at $\tau = \tau_0$ while σ_0 denotes surface density of the shell at R_0 . Using the above equation, mass of the shell becomes

$$M = 4\pi\sigma_0 \left(\frac{R_0^{2(k+1)}}{R^{2k}} \right). \quad (16)$$

In the following, we briefly discuss the dynamics of thin-shell using equations of motion.

3.1 The Schwarzschild Black Hole

The effective potential for Schwarzschild BH is given by

$$V_{eff1}(R) = -1 + \frac{M^2}{R^2} + \frac{2m_{\pm}}{R}. \quad (17)$$

The corresponding equations of motion of the shell becomes

$$\dot{R} = \pm \left[1 - \frac{M^2}{R^2} - \frac{2m_{\pm}}{R} \right]^{\frac{1}{2}}, \quad (18)$$

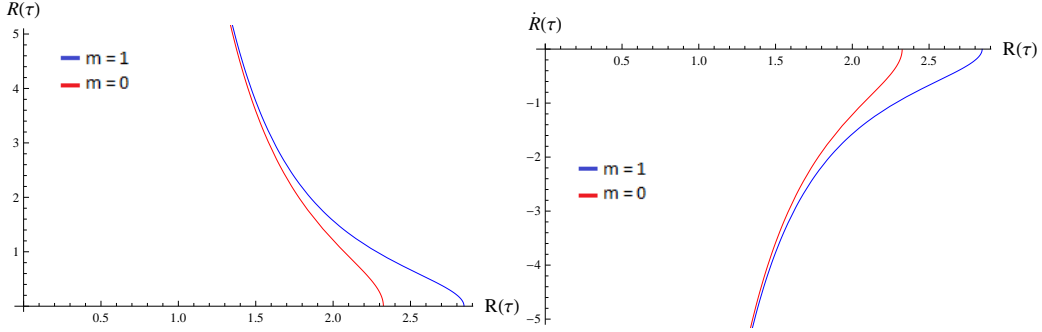


Figure 1: Behavior of thin-shell velocity corresponding to R for Schwarzschild BH with $R_0 = \sigma_0 = k = 1$.

here \pm represents expansion and collapse of thin-shell. In Figure 1, the left and right graphs describe the shell velocity for $\dot{R} > 0$ and $\dot{R} < 0$, respectively. The expansion (collapse) of the scalar shell is shown in left (right) graph, while blue and red curves correspond to interior and exterior regions. These graphs indicate that thin-shell velocity decreases positively (left plot) and increases negatively (right plot). Also, it is found that the velocity of interior region is greater than the exterior.

3.2 The Kerr Black Hole

For Kerr BH, the effective potential takes the following form

$$\begin{aligned}
 V_{eff2}(R) = & \left\{ B \left(B - \frac{AM^2}{R^2} \right) (A^2 F_{\pm} (a^2 + R^2) + 2a^2 m_{\pm} R \sin^2 \theta \right. \\
 & \times (AF_{\pm} + 8m_{\pm} R)) \} \{ (A^3 B F_{\pm} (a^2 + R^2) + 2ARa^2 m_{\pm} \\
 & \times \left(ABF_{\pm} - \frac{8Am_{\pm}M^2}{R} + 8BmR \right) \sin^2 \theta \}^{-1}. \quad (19)
 \end{aligned}$$

In this case, the respective equations of motion becomes

$$\begin{aligned}
 \dot{R} = & \pm \left[- \left\{ B \left(B - \frac{AM^2}{R^2} \right) (A^2 F_{\pm} (a^2 + R^2) + 2a^2 m_{\pm} R \sin^2 \theta \right. \right. \\
 & \times (AF_{\pm} + 8m_{\pm} R)) \} \{ (A^3 B F_{\pm} (a^2 + R^2) + 2ARa^2 m_{\pm} \\
 & \times \left. \left. \left(ABF_{\pm} - \frac{8Am_{\pm}M^2}{R} + 8BmR \right) \sin^2 \theta \right\}^{-1} \right]^{\frac{1}{2}}. \quad (20)
 \end{aligned}$$

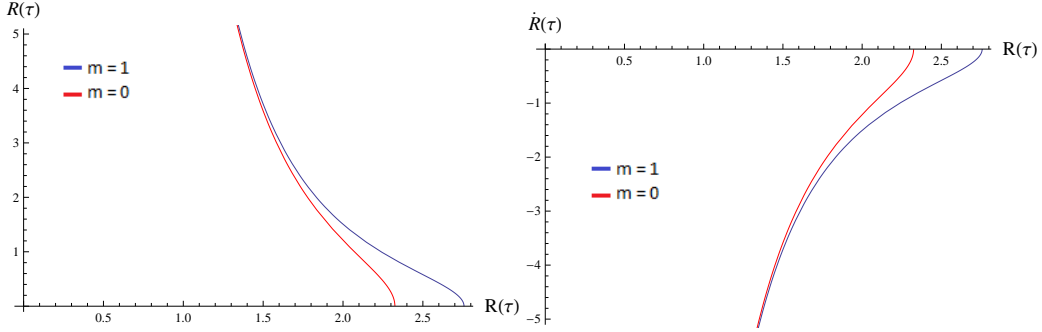


Figure 2: Behavior of thin-shell velocity corresponding to R for Kerr BH with $R_0 = \sigma_0 = k = a = 1$.

The plots for shell's velocity is shown in Figure 2. It is observed that the behavior of velocity in the presence of rotation parameter remains the same as for the Schwarzschild BH.

3.3 The Kerr-Newmann Black Hole

This BH is a generalization of the Kerr BH. The corresponding effective potential is

$$\begin{aligned}
V_{eff3}(R) &= - \left\{ B \left(B - \frac{4AM^2}{R^2} \right) (-A^2 F_{\pm} (a^2 + R^2) + a^2 (Q^2 - 2m_{\pm}R) \right. \\
&\times (AF_{\pm} - 4Q^2 + 8m_{\pm}R) \sin^2 \theta) \} \{ (A^3 B F_{\pm} (a^2 + R^2) - a^2 A \\
&\times \left(\frac{16A (Q^2 - 2m_{\pm}R) M^2}{R^2} + B (AF_{\pm} - 4Q^2 + 8m_{\pm}R) \right) \\
&\times (Q^2 - 2m_{\pm}R) \sin^2 \theta \}^{-1}. \tag{21}
\end{aligned}$$

The equations of motion for this BH takes the form

$$\begin{aligned}
\dot{R} &= \pm \left[\left\{ B \left(B - \frac{4AM^2}{R^2} \right) (-A^2 F_{\pm} (a^2 + R^2) + a^2 (Q^2 - 2m_{\pm}R) \right. \right. \\
&\times (AF_{\pm} - 4Q^2 + 8m_{\pm}R) \sin^2 \theta) \} \{ (A^3 B F_{\pm} (a^2 + R^2) - a^2 A \\
&\times \left(\frac{16A (Q^2 - 2m_{\pm}R) M^2}{R^2} + B (AF_{\pm} - 4Q^2 + 8m_{\pm}R) \right) \\
&\times (Q^2 - 2m_{\pm}R) \sin^2 \theta \}^{-1} \Big]^{\frac{1}{2}}. \tag{22}
\end{aligned}$$

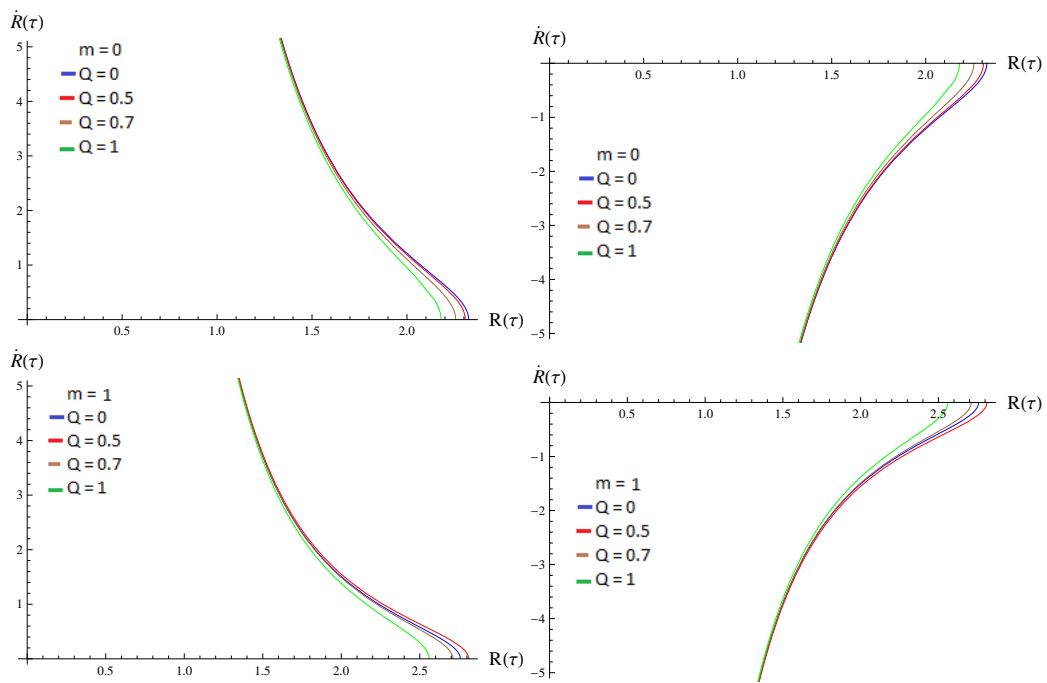


Figure 3: Behavior of thin-shell velocity corresponding to R for Kerr-Newmann BH with $R_0 = \sigma_0 = k = a = 1$.

Figure 3 (upper panel is for exterior while lower is for interior region) indicates that the velocity of thin-shell depends on charge but there is no contribution of rotation parameter. When we increase charge, the velocity decreases positively for both spacetimes as shown in the left plot of upper as well as lower panel. It is observed that velocity increases negatively for these geometries as shown in the right plot of upper as well as lower panel.

3.4 Dynamics of Scalar Shell

Here we examine the dynamical behavior of the scalar shell. For this purpose, we use a transformation $\left(u_a = \frac{\psi_{,a}}{\sqrt{\psi_{,b}\psi^{,b}}}\right)$ [19], which relates surface energy density and pressure of a perfect fluid with potential function $V(\psi)$ and derivative of the scalar field. The corresponding surface energy density and pressure are obtained as follows

$$\sigma = -\frac{1}{2} [\psi_{,b}\psi^{,b} - 2V(\psi)], \quad p = -\frac{1}{2} [\psi_{,b}\psi^{,b} + 2V(\psi)], \quad (23)$$

where $V(\psi) = M^2\psi^2$. The stress-energy tensor in terms of scalar field is defined as

$$S_{ij} = \nabla_i\psi\nabla_j\psi - \eta_{ij} \left[\frac{1}{2}(\nabla\psi)^2 - V(\psi) \right].$$

Since, the induced metric is a function of proper time τ , so ψ depends on τ . Consequently, Eq.(23) yields

$$\sigma = \frac{1}{2} [\dot{\psi}^2 + 2V(\psi)], \quad p = \frac{1}{2} [\dot{\psi}^2 - 2V(\psi)]. \quad (24)$$

The total mass of the shell ($M = A\sigma$) in terms of scalar field is defined as

$$M = 4\pi R^2\sigma = 2\pi R^2[\dot{\psi}^2 + 2V(\psi)]. \quad (25)$$

Inserting Eqs.(24) and (25) in (14), we obtain

$$\ddot{\psi} + \frac{2\dot{R}}{R}\dot{\psi} + \frac{\partial V}{\partial\psi} = 0. \quad (26)$$

This is a well-known Klein-Gordon (KG) equation and its representation in shell coordinate system is $\square\psi + \partial V/\partial\psi = 0$.

In order to analyze the dynamical behavior of spherical scalar shell, we solve KG as well as energy conservation equation simultaneously for $\psi(\tau)$ and $R(\tau)$. The effective potential for the Schwarzschild, Kerr and Kerr-Newmann BHs in terms of scalar field are obtained as

$$V_{eff1}(R) = -1 + \frac{2m_{\pm}}{R} + 4\pi^2 R^2 \left[\dot{\psi}^2 + 2V(\psi) \right]^2, \quad (27)$$

$$\begin{aligned} V_{eff2}(R) &= \left\{ B \left(B - 4A\pi^2 R^2 \left[\dot{\psi}^2 + 2V(\psi) \right]^2 \right) (A^2 F_{\pm} (a^2 + R^2) + 2a^2 \right. \\ &\times (AF_{\pm} + 8m_{\pm}R) m_{\pm} R \sin^2 \theta) \left. \right\} \left\{ (A^3 B F_{\pm} (a^2 + R^2) + 2a^2 \right. \\ &\times (ABF_{\pm} - 32Am_{\pm}\pi^2 R^3 [\dot{\psi}^2 + 2V(\psi)]^2 + 8BmR) \\ &\times m_{\pm} AR \sin^2 \theta) \left. \right\}^{-1}, \end{aligned} \quad (28)$$

$$\begin{aligned} V_{eff3}(R) &= - \left\{ B \left(B - 16\pi^2 AR^2 \left[\dot{\psi}^2 + 2V(\psi) \right]^2 \right) (-A^2 F_{\pm} (a^2 + R^2) \right. \\ &+ a^2 (Q^2 - 2m_{\pm}R) (AF_{\pm} - 4Q^2 + 8m_{\pm}R) \sin^2 \theta) \left. \right\} \left\{ (A^3 B F_{\pm} \right. \\ &\times (a^2 + R^2) - a^2 A \left(64\pi^2 A (Q^2 - 2m_{\pm}R) R^2 \left[\dot{\psi}^2 + 2V(\psi) \right]^2 \right. \\ &+ B (AF_{\pm} - 4Q^2 + 8m_{\pm}R)) (Q^2 - 2m_{\pm}R) \sin^2 \theta) \left. \right\}^{-1}. \end{aligned} \quad (29)$$

Equations (8) and (26) can be solved numerically for $m_- = 0$ and $m_+ = R_0 = \sigma_0 = k = M = 1$. Figure 4 indicates the dynamical behavior of shell corresponding to Schwarzschild, Kerr and Kerr-Newmann BHs. Here, each graph describes the motion of scalar shell through upper and lower curves indicating the expanding and collapsing behavior, respectively. For Kerr BH, it is found that the increase in rotation parameter leads to enhancement of expansion as well as collapse rate. In case of Kerr-Newmann BH, we analyze that the presence of charge and rotation parameters decreases the expansion and collapse rate.

Now, we study the dynamical behavior of scalar shell for massless as well as massive scalar field.

3.4.1 Massless Scalar Shell

Here we analyze the dynamical behavior of shell in the absence of scalar potential field ($V(\psi)$), i.e., massless scalar field. In this case, we do not need different EoS because the vanishing of ($V(\psi)$) leads to a direct relation

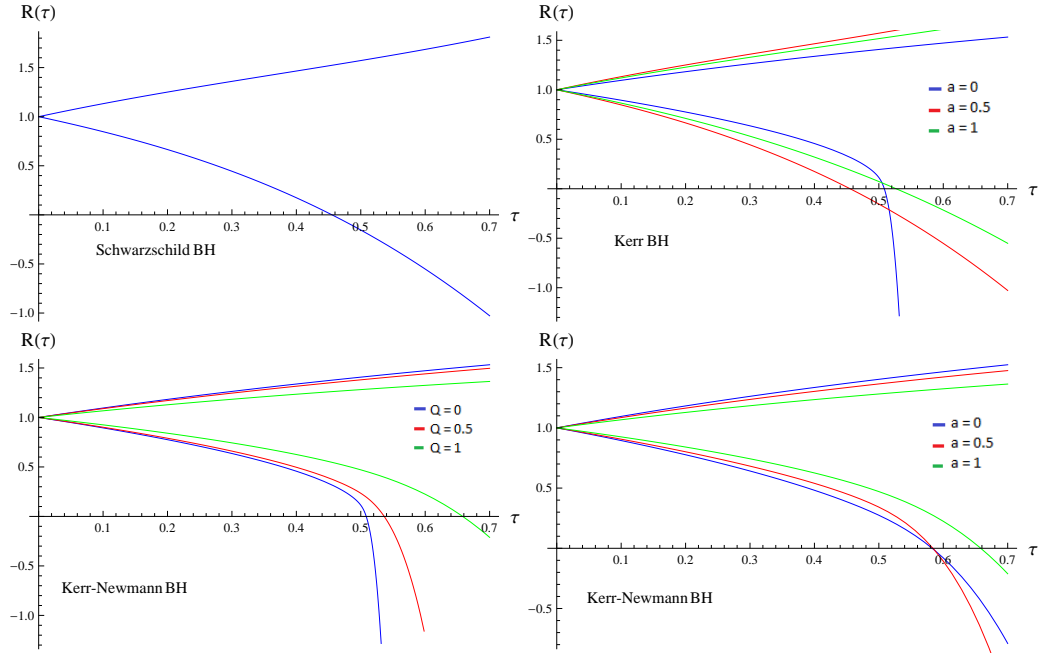


Figure 4: Behavior of shell's radius with scalar field.

between pressure and surface density ($p = \sigma$). Using the condition $V(\psi) = 0$, the KG equation can be written as $\ddot{\psi} + \frac{2\dot{R}}{R}\dot{\psi} = 0$ and its integration leads to $\dot{\psi} = \frac{\lambda}{R^2}$, where λ is an integrating constant. The equations of motion for

Schwarzschild, Kerr and Kerr-Newmann BHs become

$$\dot{R}^2 = 1 - \frac{2m_{\pm}}{R} - \frac{4\pi^2\lambda^4}{R^6}, \quad (30)$$

$$\begin{aligned} \dot{R}^2 &= - \left\{ B \left(B - \frac{4A\pi^2\lambda^4}{R^6} \right) (A^2F_{\pm} (a^2 + R^2) + 2a^2m_{\pm}R \sin^2 \theta \right. \\ &\times (AF_{\pm} + 8m_{\pm}R)) \} \{ (A^3BF_{\pm} (a^2 + R^2) + 2ARa^2m_{\pm} \\ &\times \left(ABF_{\pm} - \frac{32\pi^2Am_{\pm}\lambda^4}{R^5} + 8BmR \right) \sin^2 \theta \}^{-1}, \end{aligned} \quad (31)$$

$$\begin{aligned} \dot{R}^2 &= \left\{ B \left(B - \frac{16A\pi^2\lambda^4}{R^6} \right) (-A^2F_{\pm} (a^2 + R^2) + a^2 (Q^2 - 2m_{\pm}R) \right. \\ &\times (AF_{\pm} - 4Q^2 + 8m_{\pm}R) \sin^2 \theta) \} \{ (A^3BF_{\pm} (a^2 + R^2) - a^2A \\ &\times \left(\frac{64\pi^2A(Q^2 - 2m_{\pm}R)\lambda^4}{R^6} + B (AF_{\pm} - 4Q^2 + 8m_{\pm}R) \right) \\ &\times (Q^2 - 2m_{\pm}R) \sin^2 \theta \}^{-1}. \end{aligned} \quad (32)$$

The corresponding effective potential are

$$V_{eff1}(R) = -1 + \frac{2m_{\pm}}{R} + \frac{4\pi^2\lambda^4}{R^6}, \quad (33)$$

$$\begin{aligned} V_{eff2}(R) &= \left\{ B \left(B - \frac{4A\pi^2\lambda^4}{R^6} \right) (A^2F_{\pm} (a^2 + R^2) + 2a^2m_{\pm}R \sin^2 \theta \right. \\ &\times (AF_{\pm} + 8m_{\pm}R)) \} \{ (A^3BF_{\pm} (a^2 + R^2) + 2ARa^2m_{\pm} \\ &\times \left(ABF_{\pm} - \frac{32\pi^2Am_{\pm}\lambda^4}{R^5} + 8BmR \right) \sin^2 \theta \}^{-1}, \end{aligned} \quad (34)$$

$$\begin{aligned} V_{eff3}(R) &= - \left\{ B \left(B - \frac{16A\pi^2\lambda^4}{R^6} \right) (-A^2F_{\pm} (a^2 + R^2) + (Q^2 - 2m_{\pm}R) \right. \\ &\times (AF_{\pm} - 4Q^2 + 8m_{\pm}R) a^2 \sin^2 \theta) \} \{ (A^3BF_{\pm} (a^2 + R^2) - a^2A \\ &\times \left(\frac{64\pi^2A(Q^2 - 2m_{\pm}R)\lambda^4}{R^6} + B (AF_{\pm} - 4Q^2 + 8m_{\pm}R) \right) \\ &\times (Q^2 - 2m_{\pm}R) \sin^2 \theta \}^{-1}. \end{aligned} \quad (35)$$

The radius of shell and effective potential for massless scalar field are plotted in Figures 5-7. Figure 5 shows increasing and decreasing behavior of

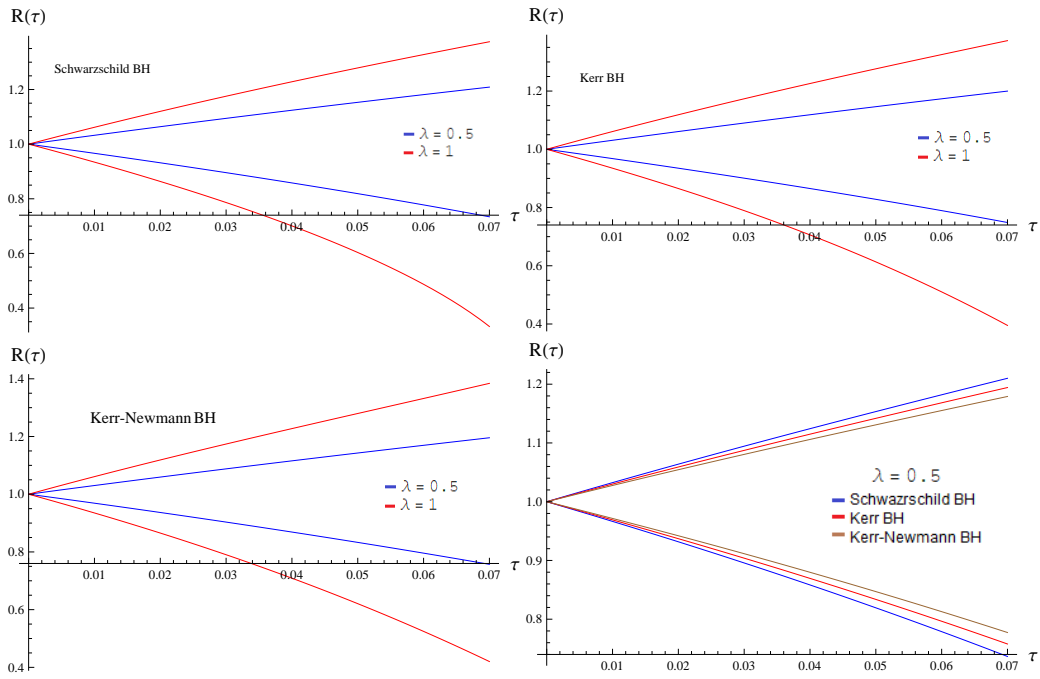


Figure 5: Behavior of shell's radius with massless scalar field.

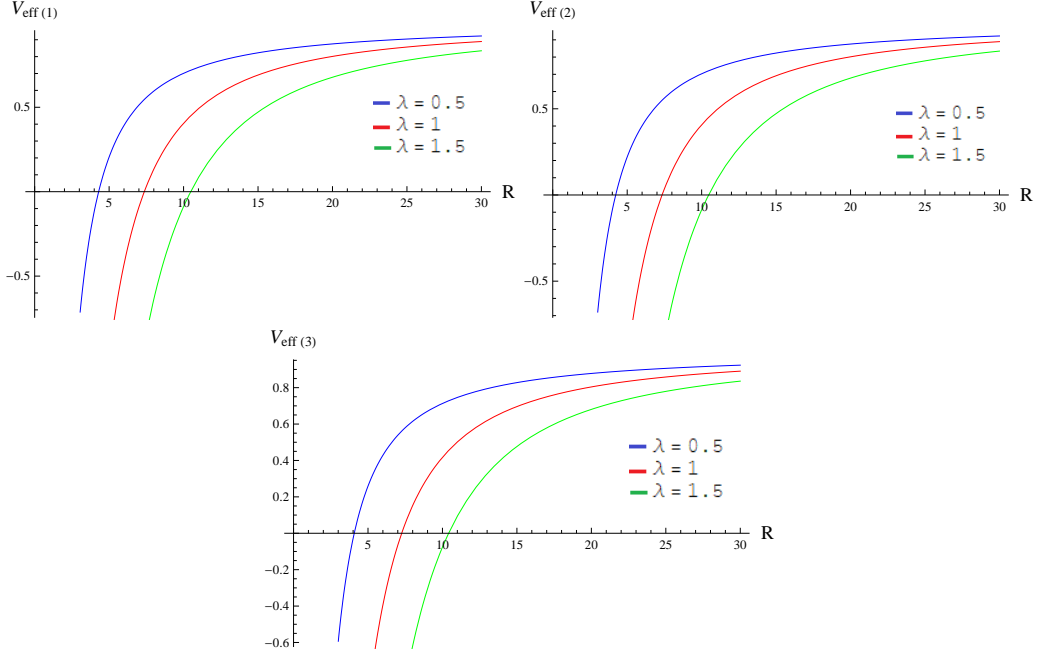


Figure 6: Plots of V_{eff} versus R for the interior region.

radius which leads to expansion and collapse, respectively. It is also observed that the rate of expansion as well as collapse increases by increasing λ . The right plot of lower panel shows that the contribution of charge and rotation parameters decreases the collapse as well as expansion rate. Figures **6** and **7** represent the dynamics of massless scalar shell through effective potential. These plots describe the expansion ($V_{eff} > 0$), collapse ($V_{eff} < 0$) and saddle points ($V_{eff} = 0$) of massless scalar shell. Figures **6** and **7** show that the scalar shell has the same behavior of expansion, collapse as well as saddle points. It is shown that the dynamical behavior of shell decreases by enhancing charge and rotation parameters.

3.4.2 Massive Scalar Shell

In this case, we discuss the dynamics of scalar shell through massive scalar field, i.e., $V(\psi) = M^2\psi^2$. From Eq.(24), we find the potential function and massive scalar field given as

$$\dot{\psi}^2 = \sigma + p, \quad 2V(\psi) = p - \sigma. \quad (36)$$

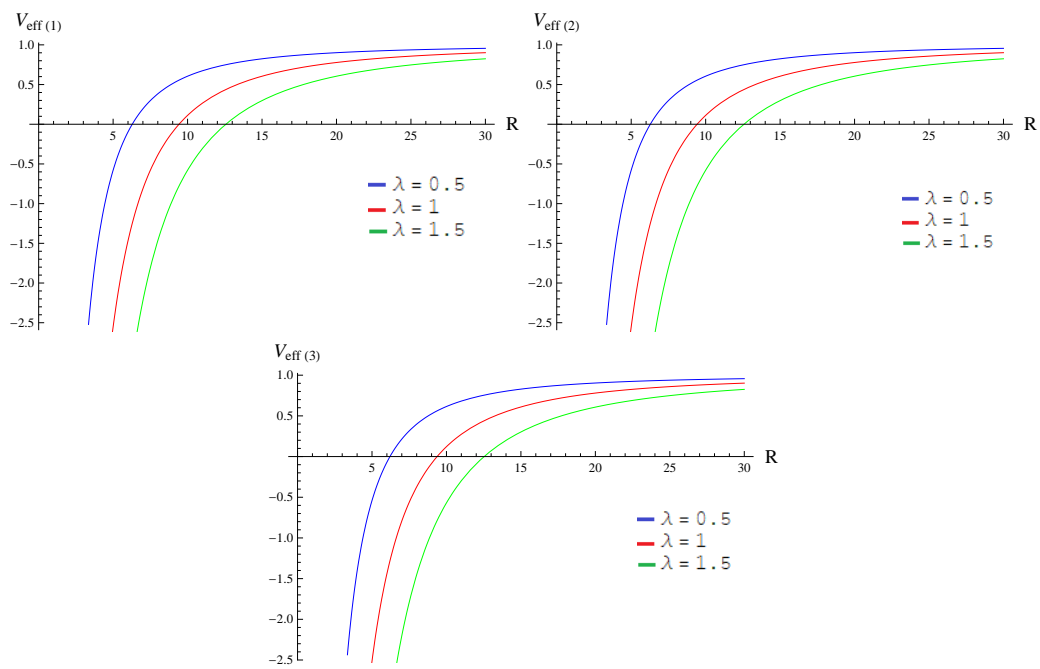


Figure 7: Plots of V_{eff} versus R for the exterior region.

We consider surface pressure as explicit function of R , i.e., $p = p_0 e^{-\gamma R}$, where γ and p_0 are constants. Using Eq.(14) alongwith the value of p , we find

$$\sigma = \frac{\omega}{R^2} + \frac{2(1 + \gamma R)p_0 e^{-\gamma R}}{\gamma^2 R^2}, \quad (37)$$

where ω is an integration constant. Using the values of energy density and surface pressure in Eq.(36), we obtain

$$V(\psi) = \frac{\omega}{2R^2} - \frac{p_0 e^{-\gamma R}}{2} \left(1 - \frac{2(1 + \gamma R)}{\gamma^2 R^2} \right), \quad (38)$$

$$\dot{\psi}^2 = \frac{\omega}{R^2} - p_0 e^{-\gamma R} \left(1 + \frac{2(1 + \gamma R)}{\gamma^2 R^2} \right), \quad (39)$$

which satisfy the KG equation. Using Eqs.(37)-(39) in (27)-(29), it follows that

$$V_{eff1}(R) = -1 + \frac{M^2}{R^2} + \frac{2m_{\pm}}{R}, \quad (40)$$

$$\begin{aligned} V_{eff2}(R) &= \left\{ B \left(B - \frac{AM^2}{R^2} \right) (A^2 F_{\pm} (a^2 + R^2) + 2a^2 m_{\pm} R \sin^2 \theta \right. \\ &\times (AF_{\pm} + 8m_{\pm} R)) \} \{ (A^3 B F_{\pm} (a^2 + R^2) + 2ARa^2 m_{\pm} \\ &\times \left(ABF_{\pm} - \frac{8Am_{\pm} M^2}{R} + 8BmR \right) \sin^2 \theta \}^{-1}, \end{aligned} \quad (41)$$

$$\begin{aligned} V_{eff3}(R) &= - \left\{ B \left(B - \frac{4AM^2}{R^2} \right) (-A^2 F_{\pm} (a^2 + R^2) + a^2 (Q^2 - 2m_{\pm} R) \right. \\ &\times (AF_{\pm} - 4Q^2 + 8m_{\pm} R) \sin^2 \theta) \} \{ (A^3 B F_{\pm} (a^2 + R^2) - a^2 A \\ &\times \left(\frac{16A(Q^2 - 2m_{\pm} R) M^2}{R^2} + B (AF_{\pm} - 4Q^2 + 8m_{\pm} R) \right) \\ &\times (Q^2 - 2m_{\pm} R) \sin^2 \theta \}^{-1}. \end{aligned} \quad (42)$$

Also, the mass of shell can be expressed as

$$M = 4\pi R^2 \sigma = 4\pi \omega + \frac{8\pi p_0 e^{-\gamma R}}{\gamma^2} (1 + \gamma R). \quad (43)$$

Figures **8-10** indicate the behavior of shell's radius as well as effective potential for massive scalar field for $m_- = 0$ and $m_+ = R_0 = \sigma_0 = \omega = \gamma =$

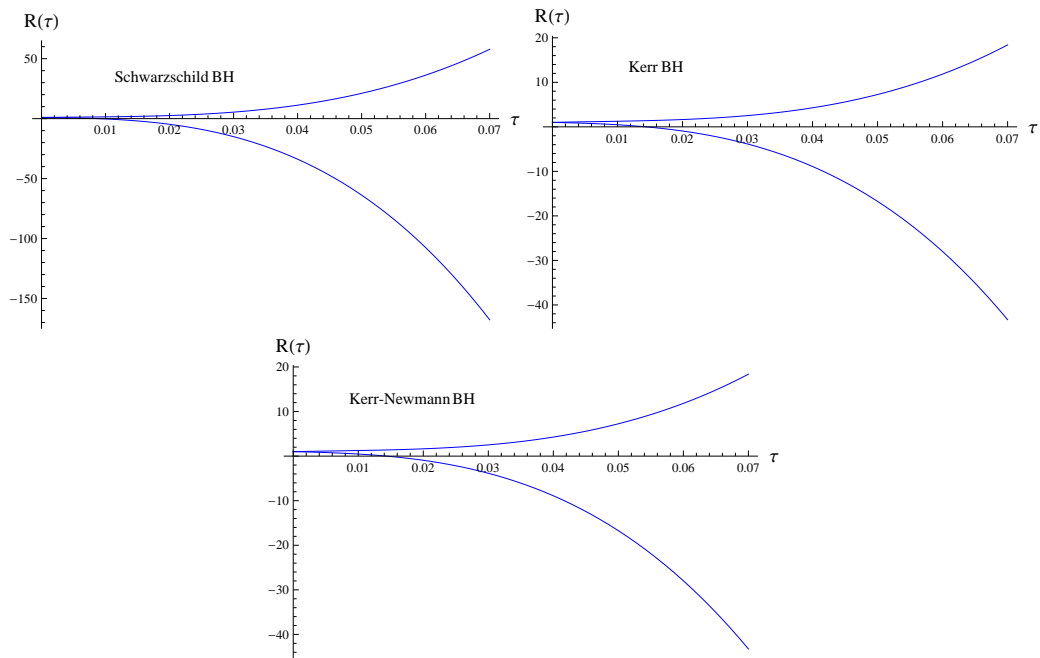


Figure 8: Behavior of shell's radius with massive scalar shell.

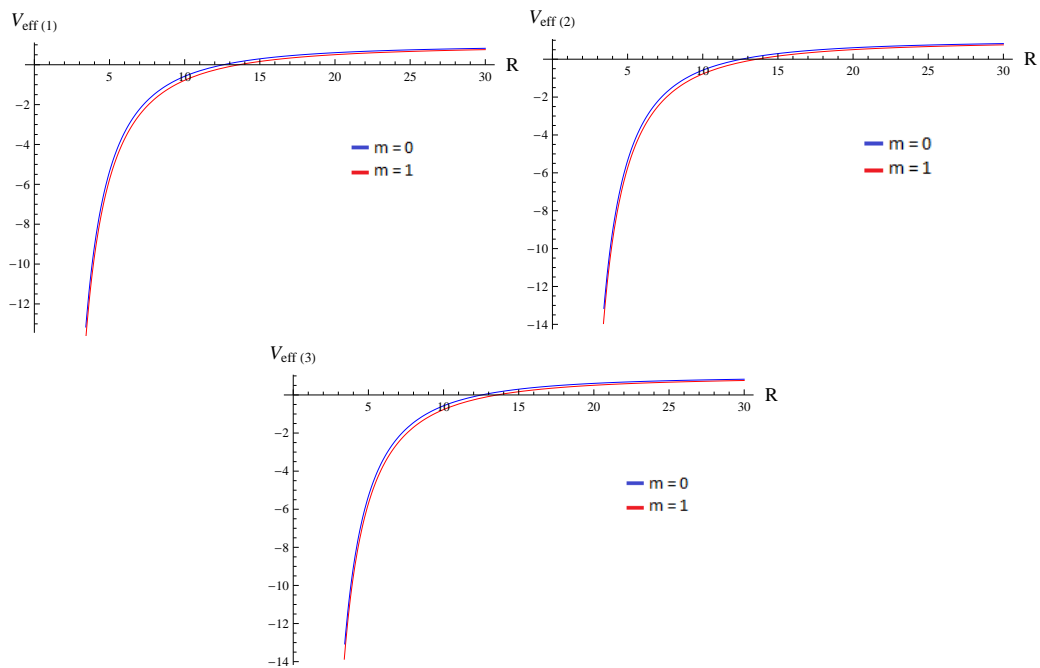


Figure 9: Plots of V_{eff} versus R for massive case when $\omega = 1$.

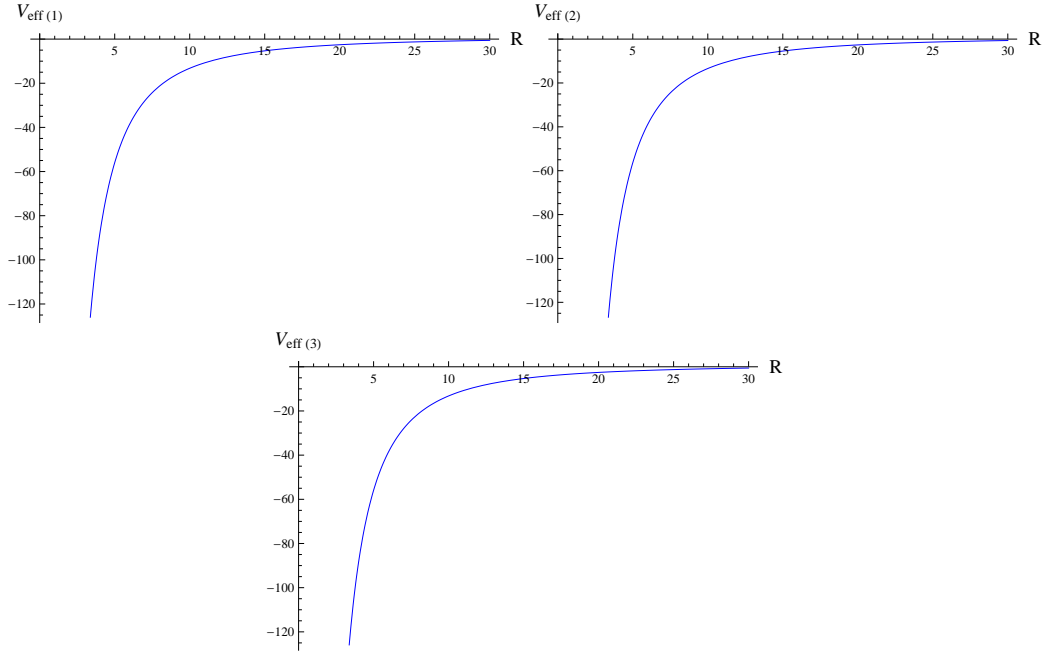


Figure 10: Plots of V_{eff} versus R for massive case when $\omega = 3$.

$Q = a = 1$. In Figure 8, the upper curve represents the expansion of scalar shell while the lower curve shows collapse. Figure 9 shows that the effective potential for massive scalar field leads to expansion, collapse as well as saddle points for $\omega \in (-2, 2)$. It is also found that $-2 \geq \omega \geq 2$ leads the shell to collapse (negative effective potential) only (Figure 10). For massive scalar field, we find that the effective potential exhibits similar behavior (expansion, collapse and saddle point) for all values of free parameters.

4 Final Remarks

In this paper, we have studied the dynamics of scalar shell for a class of BHs using Israel thin-shell formalism. For this purpose, we have formulated the equations of motion which leads to the behavior of shell's velocity. We have then investigated the dynamics of scalar shell for massless and massive scalar fields. The results can be summarized as follows.

- The motion of scalar shell shows expanding as well as collapsing be-

havior of the shell (Figures 1-4). It is found that shell's velocity has similar behavior for all considered BHs. For the Kerr-Newmann BH, it is analyzed that the velocity of shell decreases by enhancing charge parameter (Figure 3). We have obtained that the rate of expansion and collapse for Schwarzschild BH is greater than the Kerr and Kerr-Newmann BHs (Figure 4).

- For massless scalar field, it is observed that the presence of charge and rotation parameters affect the dynamical behavior of shell's radius. For the Kerr and Kerr-Newmann BHs, expansion as well as collapse rate is small as compared to the Schwarzschild BH (Figure 5). The behavior of effective potential indicates the expansion, collapse as well as the stable points (Figures 6-7). For both interior and exterior spacetimes, expansion and collapse rates are decreased as λ increases (Figures 6 and 7).
- For massive scalar field, it is shown that the radius of shell either expands or undergoes collapse. We have found that Schwarzschild BH exhibits more expansion and collapse as compared to Kerr and Kerr-Newmann BHs. This describes that the contribution of charge and rotation parameters decreases these phenomena (Figure 8). It is found that V_{eff} shows expansion as well as collapse of thin-shell for $\omega \in (-2, 2)$ while it indicates only collapse for other values of ω (Figures 9 and 10). It is observed that the behavior of effective potential for three BHs overlaps for all values of charge as well as rotation parameter.

We conclude that the dynamical evolution of scalar shell can be expressed through continuous expansion, collapse and stable configuration.

References

- [1] Wheeler, J.A.: Phys. Rev. **97**(1955)511; Brill, D.R. and Wheeler, J.A.: Phys. Rev. **105**(1957)1662.
- [2] Bergmann, Q. and Leipnik, R.: Phys. Rev. **107**(1957)1157.
- [3] Damour, T. and Polyakov, A.M.: Gen. Relativ. Gravit. **26**(1994)1171.

- [4] Harada, T., Chiba, T., Nakao, K. and Nakamura, K.: Phys. Rev. D **55**(1997)2029.
- [5] Kaup, D.J.: Phys. Rev. **172**(1968)1331.
- [6] Ruffini, R. and Bonazzola, S.: Phys. Rev. **187**(1969)1767.
- [7] Seidel, E. and Suen, W.: Phys. Rev. D **42**(1990)384.
- [8] Jetzer, P.: Phys. Rep. **220**(1992)163.
- [9] Choptuik, M.W.: Phys. Rev. Lett. **70**(1993)9; Evans, C.R. and Coleman, J.S.: Phys. Rev. Lett. **72**(1994)1782; Christodoulou, D.: Ann. Math. **140**(1994)607; Malec, E.: Class. Quantum Grav. **13**(1995)1849; Gundlach, C.: Phys. Rev. Lett. **75**(1995)3214; Bardy, P.R.: Class. Quantum Grav. **11**(1996)1255.
- [10] Siebel, F., Font, J.A. and Papadopoulos, P.: Phys. Rev. D **65**(2001)024021.
- [11] Bhattacharya, S., Goswami, R. and Joshi, P.S.: arXiv:gr-qc/0410144.
- [12] Israel, W.: Nuovo Cimento B **44**(1966)1; *ibid.* **48**(1967)463.
- [13] Lake, K.: Phys. Rev. D **19**(1979)2847; Lake, K. and Wevrick, R.: Can. J. Phys. **64**(1986)165; Khorrami, M. and Mansouri, R.: Phys. Rev. D **44**(1991)557; Mansouri, R. and Khorrami, M.: J. Math. Phys. **37**(1996)5672.
- [14] De La Cruz, V. and Israel, W.: Nuovo Cimento A **51**(1967)744.
- [15] Kuchar, K.: Czechoslovak J. Phys. B **18**(1968)435.
- [16] Chase, J.E.: Nuovo Cimento B **67**(1970)136.
- [17] Boulware, D.G.: Phys. Rev. D **8**(1973)2363.
- [18] Núñez, D.: Astrophys. J. **482**(1997)963.
- [19] Núñez, D., Quevedo, H. and Salgado, M.: Phys. Rev. D **58**(1998)083506.
- [20] Pereira, P.R.C.T. and Wang, A.: Phys. Rev. D **62**(2000)124001.

- [21] Sharif, M. and Ahmad, Z.: Int. J. Mod. Phys. A **23**(2008)181 ; Sharif, M. and Iqbal, K.: Mod. Phys. Lett. A **24**(2009)1533; Sharif, M. and Abbas, G.: Gen. Relativ. Gravit. **43**(2011)1179.
- [22] Sharif, M. and Abbas, G.: Gen. Relativ. Gravit. **44**(2012)2353.
- [23] Sharif, M. and Iftikhar, S.: Astrophys. Space Sci. **356**(2015)89.